Control of Power Electronics-Based Synchronous Generator for the Integration of Renewable Energies into the Power Grid

Majid Mehrasa [a], Edris Pouresmaeil [b,*], Amir Sepehr [b], Bahram Pournazarian [b], and João P. S. Catalão [c,*]

[a] C-MAST, University of Beira Interior, 6201-001 Covilhã, Portugal

[b] Department of Electrical Engineering and Automation, Aalto University, 02150 Espoo, Finland

[c] Faculty of Engineering of the University of Porto and INESC TEC, 4200-465 Porto, Portugal

* Corresponding authors: Edris Pouresmaeil (edris.pouresmaeil@gmail.com) and João P. S. Catalão (catalao@ubi.pt)

Abstract—This paper addresses a single synchronous controller (SSC) for interfaced converters with high penetration of renewable energy resources (RERs) into a low inertia power grid. The SSC is modelled based on a comprehensive dependence between each operative feature of a synchronous generator (SG) and a power electronics converter. This can properly improve the performance of the power grid in such scenarios in which large-scale penetration of RERs are detected. The main contribution of this paper is representing an exhaustive relation between active components of the proposed SSC and SG features which enables the proposed SSC-based interfaced converter to more accurately mimic the behaviour of SGs during active power generating along with providing controllable inertia. Due to containing sufficient decoupling, both components of the proposed SSC have no impact on each other, also the proposed SSC has a superior operational flexibility within a wide range of inertia from very low to high values. Thus, two closed-loop control systems are considered to separately analyse the characteristic effects of SGs in active and reactive power sharing apart from the power grid stability challenges. In addition, the impacts of active power variations on reactive power are subsequently evaluated. To further analyse the operation of the system, the effects of the virtual mechanical power (VMP) error embedded in the SSC are considered as an alternative option for assessing the power grid stability. Also, the variations of the virtual angular frequency (VAF) error are carefully deliberated for more considerations associated with the active and reactive power performance of the SSC. Simulation results are presented to demonstrate the high performance of the SSC in the control of the power electronics-based SG when high-penetration renewable energy sources are integrated into the low inertia power grid.

Keywords—Single synchronous controller; low inertia power grid; renewable energy resources; virtual mechanical power; virtual angular frequency.

I. Nomenclature

Abbreviation

RERs	Renewable Energy Resources
VAF	Virtual Angular Frequency
VMP	Virtual Mechanical Power
SSC	Single Synchronous Controller
SG	Synchronous Generator
DESS	Distributed Energy Storage System
VSM	Virtual Synchronous Machine
PV	Photovoltaic
PCC	Point of Common Coupling
LPF	Low Pass Filter

Variables

i_{dq}	Currents of Converter in dq reference frame
v_{dq}	Voltages at PCC in dq reference frame
v_{dc}	dc-Link Voltage
u_{dq}	Switching Functions
i_{dc}	dc-Link Current
P	The Active Power of interfaced converter
Q	The Reactive Power of interfaced converter
P_{c2}	dc-Link Current Based Power
P_d	d-Component Power
P_{dq}	Combined Power
P_m	Mechanical Power
ω	Angular Frequency
ΔP	Active Power Error
ΔP_m	VMP Error
$\Delta \omega_m$	VAF Error
ΔQ	Reactive Power Error
P^*	Reference Active Power

P_m^*	Reference VMP
ω^*	Reference Angular Frequency

Parameters

L	The Inductance of interfaced converter
R	The Resistance of interfaced converter
L_s	The Inductance of Power Grid
R_s	The Resistance of Power Grid
C	dc-Link Capacitor
J	Low-Value Inertia
ω_1, ω_2	LPF Coefficients
$k_{p\omega}$, $k_{i\omega}$	Coefficients of VAF Error Controller
k_{pp}, k_{ip}	The Controller Coefficients of Active Power Component
k_{pq}, k_{iq}	The Controller Coefficients of Reactive Power Component
α, β	Decoupled Factors of Closed- Loop Descriptions

II. Introduction

Due to the important role of distributed generation technology especially based on renewable energy resources (RERs) in power systems, numerous researches have been carried out to further investigate the concerns associated with unstable operation of power grid under high penetration of RERs in recent years [1]-[2]. In some studies, authors focused on using distributed energy storage systems (DESSs) for encountering stability issues by designing optimized supervisory and advanced controllers for large-scale DESSs with the aim of reliable and stable integration of RERs into the power grid [3]-[6]. In some recent studies, in order to compensate the voltage rise of the power grid caused by the excess photovoltaic (PV) sources, reactive power based controllers, designed for the interfaced converters in DG units, have been proposed [7]-[10]. Moreover, several control strategies have been proposed to overcome these challenges by emulating the inherent features of SGs and considering stability assessments of the power grid with high penetration of RER in [11]-[14].

In [15], two features of SG i.e. the inertia and damping power have been placed in the final proposed controller in order to regulate the frequency-amplitude and the power flow via/of the energy storage. In addition, the optimization of controller parameters was continuously executed through self-tuning algorithms. With the aim of preventing unstable operation of a weak AC-system integration due to a standard PLL, a power synchronization control technique based on the internal synchronization mechanism of a synchronous machine is proposed in [16]. In [17], a short-term energy buffer is added to the system through the simulation of rotor inertia which named as virtual synchronous generator since it can reduce the instability problems at the system

operational level.

A synchronous power controller has been proposed in [18] for the control of grid-connected converters for integration of RERs to the power grid. Besides, inertia, damping, and flexible droop characteristics are considered to meet the connection requirements of power converters into the power grid as well as dynamics and frequency regulations. Also, for a large-scale PV power plant, a distributed voltage control scheme has been presented in [19] in order to decrease the high ramp-rate.

In [20], a self-synchronized synchronverter has been proposed which can improve operation of the synchronous controller given in [26] by reducing the complexity, increasing the performance, and decreasing the computational efforts of the controller. This improvement has been achieved by removing the synchronizing unit containing PLL which is responsible for obtaining the reference values of phase, frequency, and voltage amplitude via the grid voltage [20].

In order to provide a synchronous conventional droop-based control for power electronic converters in stand-alone and grid-connected operating mods, virtual synchronous machines based control techniques are considered in [21] by assessing the small signal responses due to characteristics of simulating inertia. Based on the simulation of a SG and a conventional droop curve, three synchronous control techniques including all the features i.e., inertia, damping, and droop characteristics are analysed in [22] and a complete comparison is performed. The virtual synchronous machine (VSM) is considered in [23] for smart grids and while the stability analysis of VSM is evaluated in [24]-[25] for its effects on power grid with high penetration of RERs.

In this paper, a single synchronous controller (SSC) is proposed based on an active and reactive power-based dynamic model with the aim of providing a stable operation for the power grid with high penetration of RERs. The controller proposed in [26] does not provide internal decoupling in its control technique. Whereas, this paper presents an operative decoupling control scheme as a contribution for the proposed SSC. On the other hand, there is no convincing relationship between the converter and SG powers in the control technique designed in [26]. A comprehensive relationship can be seen in the proposed SSC in this paper which leads to a more accurate active and reactive power sharing for compensating a broader range of grid frequency and voltage magnitude variations.

The control system designed in [27] mainly focused on wind turbine applications based on the behavior of conventional SGs. Ref. [27] has not considered the exact dynamic equations of the interfaced converter as well as the mutual relationship between interfaced converters and SGs. Also, the electrical model of the control technique in [27] is based on the converter currents. Meanwhile, the mechanical part has been written based on mechanical power, which doesn't lead to a satisfactory control technique by emulating SG behaviors, likewise, the decoupling requirement for the designed control technique is neglected in [27]. In contrast, the proposed SSC in this paper comprises more detailed features of SG for various applications. Furthermore, an accurate dynamic model of interfaced converter based on active and reactive power as well as a comprehensive relationship between SG and interfaced converter are applied for designing the proposed SSC leading to a more appropriate and accurate control technique

for high penetration issue of RERs into the power grid.

Virtual synchronous control proposed in [28] has been designed based on droop control. In comparison with the droop-based virtual synchronous control in [28], more detailed features of SGs is utilized in the proposed SSC in this paper. Also, more accurate relationship between the dynamic behavior of the interfaced converter power and swing equation is applied in the proposed SSC. This, in turn, leads to a more controllable virtual inertia, faster transient response, more accurate steady state, more precise dynamic response, and finally more effective decoupling feature. The SG emulation presented in [29] adversely impacts on the θ of switching functions in the respective designed control scheme. Meanwhile, each aspect of the proposed SSC complies with SGs features results in the aforementioned superiorities.

The contributions of the proposed SSC are, 1) providing a comprehensive dependence between each feature of a SG and a power electronics converter active and reactive power, 2) the active component of the proposed SSC is completely implicated by SG features, 3) both components of the proposed SSC, due to providing sufficient decoupling, have no impact on each other and finally 4) embedding wide ranges of virtual inertia from very low to high values enhances the proposed SSC with a high operational flexibility.

The rest of this paper is organized as follows. Achieving the proposed active and reactive power based dynamic model is presented in the first subsection of Section III. Then, Section III is completed by designing the proposed SSC. In Section IV, two transfer functions are obtained to assess the effects of different parameters related to the SSC on the ability of the SSC at presenting accurate active and reactive power sharing as well as power grid stability. The evaluation of virtual mechanical power and effects of virtual angular frequency error in case of various low-value inertias are discussed in Section V. Finally, simulation results are given in Section VI and conclusions drawn in Section VII.

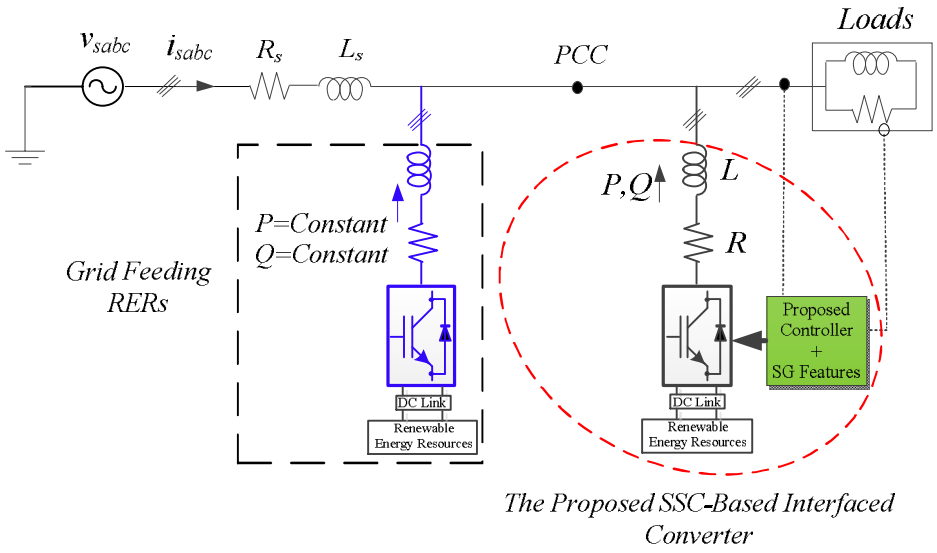

Fig. 1. General structure of the proposed model.

III. Proposed Model Presentation

The general model based on interfaced-converter for integration of large-scale RER is drawn in Fig. 1. This figure contains the power grid, loads, two types of controllable RER, and grid-feeding RER which will be discussed further in the subsequent sections. In this paper, the active power generated by renewable energy resources will be controlled by the emulated SG-based interfaced converter shown in Fig.1.

A. The Mathematical Model Presentation

The dynamic model of the proposed model in Fig. 1 should be extracted in order to draw a control technique for control of the interfaced converter for integration of large-scale RERs into the grid. By this assumption, the dynamic equations of the proposed model in *dq* reference frame can be expressed as [1]:

$$L\frac{di_d}{dt} + Ri_d - \omega L i_q - u_d v_{dc} + v_d = 0 \tag{1}$$

$$L\frac{di_q}{dt} + Ri_q + \omega L i_d - u_q v_{dc} + v_q = 0 \tag{2}$$

$$C\frac{dv_{dc}}{dt} + u_d i_d + u_q i_q + i_{dc} = 0 \tag{3}$$

The instantaneous active and reactive power of RER-based interfaced converter can be stated as $P=i_d v_d$, $Q=-i_q v_d$. By neglecting partial variations that are $v_q=0$ and $dv_d/vt=0$, a set of new active and reactive power based dynamic equations can be obtained through multiplying the d-component of the reference voltage (v_d) to (1)-(3).

$$\frac{L}{R}\frac{dP}{dt} + P + \frac{\omega L}{R}Q - u_d P_{c1} + P_d = 0 \tag{4}$$

$$\frac{L}{R}\frac{dQ}{dt} + Q - \frac{\omega L}{R}P + u_q P_{c1} - P_{dq} = 0 \tag{5}$$

$$RC\frac{dP_{c1}}{dt} + u_d P - u_q Q + P_{c2} = 0 \tag{6}$$

where, the power components in equations (4)-(6) are defined as $P_{c1}=v_{dc}v_d/R$, $P_{c2}=i_{dc}v_d$, $P_d=v_d^2/R$ and $P_{dq}=v_d v_q/R$. Two power components of P_{c1} and P_{c2} are due to dc link voltage of interfaced converter and d component of PCC voltage. The d component of PCC voltage makes the most impact on the power component of P_d that is proportional to square v_d. On the other hand, the least effect belongs to the power component of P_{dq} that can be approximately equal to zero because of existing v_q.

B. Presentation of the Proposed Single Synchronous Controller (SSC)

In this section, the proposed SSC is discussed in detail. As intended, the proposed controller should follow the inherent features of SG. Then, the proposed dynamic model along with the combination of these features is used to design the final controller for

the control of the interfaced converter. The following subsections elucidate the designing process.

B.1. The SG Characteristics Extraction

The main concerns associated with high penetration of RERs are the unstable behaviours of the voltage magnitude and the frequency of the power grid due to odd transient dynamics of interfaced converters and the lack of inertia of this kind of generators. These concerns can be noticeably decreased by considering all the properties of SGs in the structure of the control loop of the interfaced converter. As it is known, the swing equation can be stated as:

$$J\frac{d\omega}{dt}=\frac{P_m-P}{\omega} \tag{7}$$

Using the small-signal linearization for (7) and performing some simplifications, (8) can be achieved as:

$$\Delta\omega=\frac{1}{\omega^* J}\cdot\frac{\Delta P_m-\Delta P}{s+\left(P_m^*-P^*\right)/\omega^{*2}J}=\frac{\omega_1}{s+\omega_2}\left(\Delta P_m-\Delta P\right) \tag{8}$$

Considering (8), the active power variation can be written based on variations of the virtual mechanical power and virtual angular frequency as:

$$\frac{\Delta P}{s}=\frac{\Delta P_m}{s}-\left(\omega^* J+\frac{\left(P_m^*-P^*\right)}{\omega^* s}\right)\Delta\omega=\frac{\Delta P_m}{s}-\left(k_{p\omega}+\frac{k_{i\omega}}{s}\right)\Delta\omega \tag{9}$$

Equations (8) and (9) can lead to constructing the important parts of the ultimate controller consisting of all properties of the SG as shown in Fig. 2. As it is depicted, the error parts of VMP and VAF are utilized for the active power-axis of the SSC. Moreover, the scenario used for achieving the virtual angular frequency can be employed for both active and reactive-axis of the proposed ultimate SSC. In fact, the SG features involved with both active and reactive components of the proposed SSC can be obviously realized from Fig.2. In addition, the coefficients of α and β are employed to increase the decoupling features of the proposed SSC.

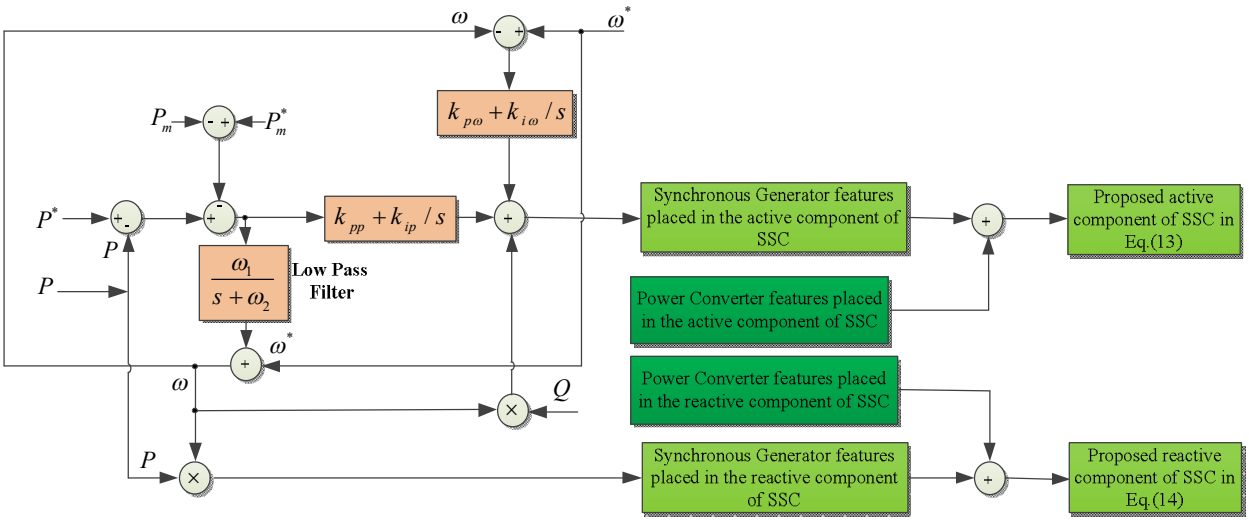

Fig. 2. The SG-based parts of the proposed single synchronous controller (SSC).

By considering a low pass filter (LPF) as $\omega_1/(s+\omega_2)$, LPF coefficients and the coefficients of PI controller associated with virtual angular frequency error can be driven as:

$$\omega_1 = \frac{1}{\omega^* J}, \omega_2 = \left(P_m^* - P^*\right)/\omega^{*2} J \tag{10}$$

$$k_{p\omega} = \omega^* J,\ k_{i\omega} = \left(P_m^* - P^*\right)/\omega^* \tag{11}$$

$$k_{pp} = 1/\omega^* J,\quad k_{ip} = \left(P_m^* - P^*\right)/\left(\omega^{*3} J^2\right) \tag{12}$$

It can be understood from (10)-(12) that all coefficients are highly dependent on inertia, reference values of active power, VMP, and VAF.

B.2. The Proposed Controller

By combining (4) and (5), and the designed SG-based parts shown in Fig. 2, the proposed SSC can be achieved as shown in Fig. 3. According to this figure, the active and reactive axis of the proposed control technique can be written as:

$$u_d = \frac{1}{P_{c1}}\left(\begin{array}{l}\left(\Delta P - \Delta P_m\right)\left(k_{pp} + k_{ip}/s\right) + \left(\Delta\omega\right)\left(k_{p\omega} + k_{i\omega}/s\right) \\ + \left(\left(\Delta P - \Delta P_m\right)\left(\frac{\omega_1}{s+\omega_2}\right) + \omega^*\right)\alpha\frac{L}{R}Q + P_d\end{array}\right) \tag{13}$$

$$u_q = \frac{-1}{P_{c1}}\left(\begin{array}{l}\Delta Q\left(k_{pq} + k_{iq}/s\right) - \\ \left(\left(\Delta P - \Delta P_m\right)\left(\frac{\omega_1}{s+\omega_2}\right) + \omega^*\right)\beta\frac{L}{R}P - P_{dq}\end{array}\right) \tag{14}$$

Equations (13) and (14) show that both d and q axis of the SSC are affected by the features of the synchronous generator. This advantage can significantly cause the added inherent features of the synchronous generator to make more contributions in operation of interfaced converter in stability of power grid with high penetration of RER. This advantage is analysed in the next sections.

IV. Operating Evaluation of the SSC

Specifying the effects of virtual SG features on synchronous operation of the interfaced converter and the power grid stability is a substantial step for evaluation of the SSC that can provide more beneficial control factors. In this section, the effects of the coefficients variations used in the structure of the SSC and also impacts of active power changes on reactive power are discussed. By performing some mathematical considerations on the active power equations (4) and (13) and also reactive power equations (5) and (14), two closed-loop diagrams based on the SSC for the active and reactive power of the interfaced converter can be achieved, as shown in Fig. 3. The performance assessment of the SSC in various conditions is presented in the following subsections.

A. The Active and Reactive Power Tracking Capabilities

As can be seen from Fig. 3, both active and reactive power and their reference values are used as the output and input of closed-loop descriptions of the SSC, respectively.

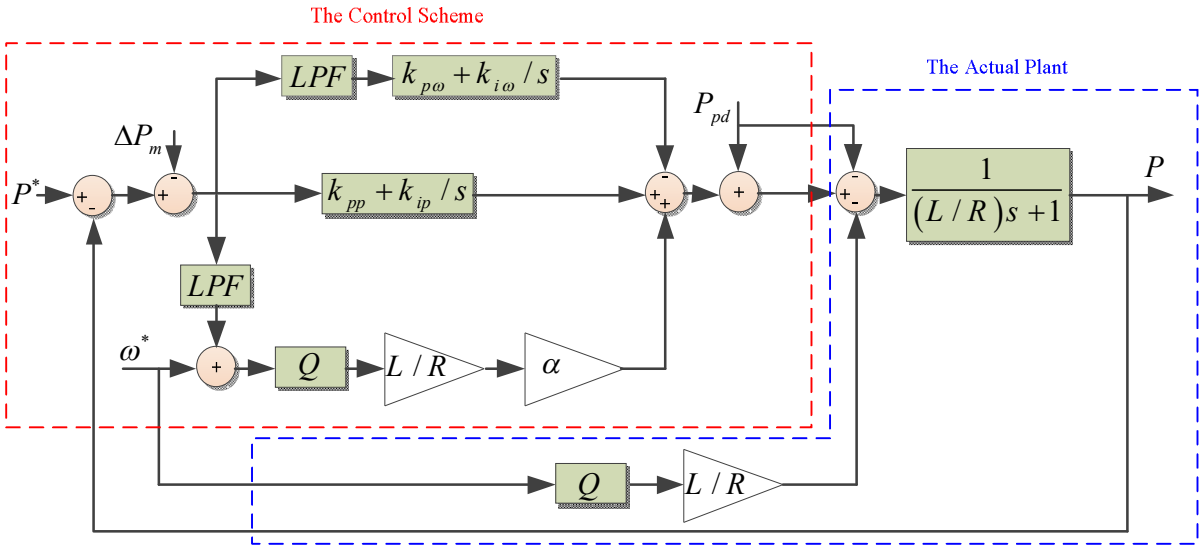

(a)

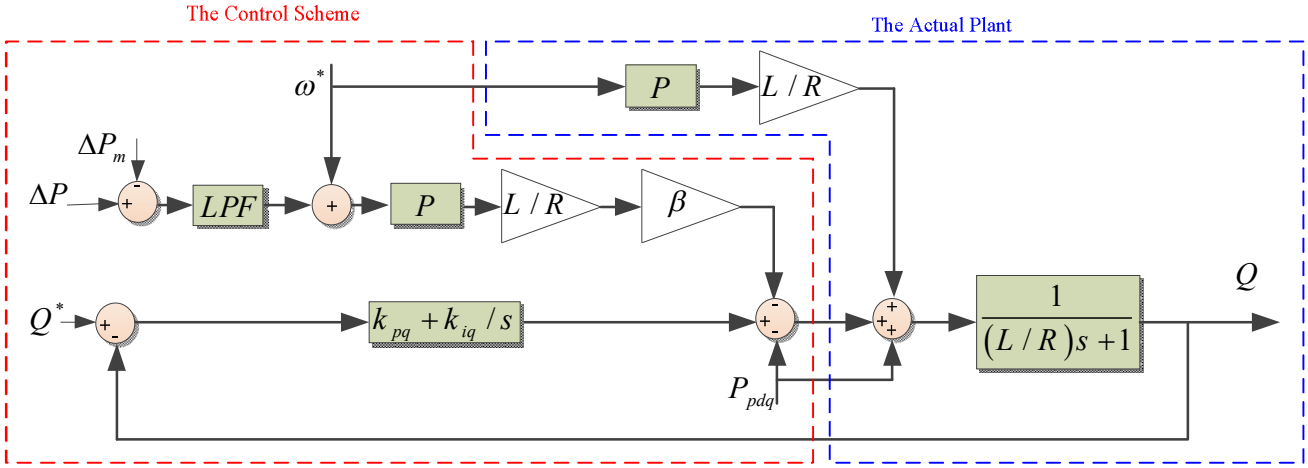

(b)

Fig. 3. The proposed single synchronous controller (SSC): (a) active power component, (b) reactive power component.

The coefficients of α and β are the decoupling factors of the closed loop descriptions that can vary the amount of decoupled relationship between the active component of the SSC and the reactive power and vice versa. In fact, these coefficients make the relationship between P and Q in the SSC. In addition, the parameters of the reactive power controller (k_{pq} and k_{iq}) are selected by the use of the trial and error method. By considering two closed-loop diagrams in Fig. 3, two transfer functions related to active and reactive power are driven as (15) and (16) as:

$$\frac{P}{P^*}=\frac{\left(\begin{array}{l}\left(\begin{array}{l}\left(Lk_{pp}/R\right)s^4+\left[\begin{array}{l}\left(L/R\right)\left(k_{ip}+k_{pp}\omega_2-\omega_1k_{p\omega}\right)\\+\left(k_{pp}\right)\left(1+k_{pq}\right)\end{array}\right]s^3\end{array}\right)\\+\left[\begin{array}{l}\left(L/R\right)\left(k_{ip}\omega_2-\omega_1k_{i\omega}\right)+\alpha\omega_1k_{pq}\dfrac{L}{R}\\\left(1+k_{pq}\right)\left(k_{ip}+k_{pp}\omega_2-\omega_1k_{p\omega}\right)+k_{pp}k_{iq}\end{array}\right]s^2\\+\left[\begin{array}{l}\left(k_{ip}\omega_2-\omega_1k_{i\omega}\right)\left(1+k_{pq}\right)+\\k_{iq}\left(k_{ip}+k_{pp}\omega_2-\omega_1k_{p\omega}\right)+\alpha\omega_1k_{iq}\left(L/R\right)\end{array}\right]s\\+\left(k_{ip}\omega_2-\omega_1k_{i\omega}\right)k_{iq}\end{array}\right)}{\left(\begin{array}{l}\left(L/R\right)^2s^5+\left(L/R\right)\left(2+k_{pp}+\left(L/R\right)\omega_2+k_{pq}\right)s^4\\+\left(\begin{array}{l}\left(L/R\right)\left(k_{pp}\omega_2+k_{ip}-k_{p\omega}\omega_1\right)+k_{pp}\left(1+k_{pq}\right)+\\\left(L/R\right)k_{iq}+\left(\left(L/R\right)\omega_2+1\right)\left(1+k_{pq}\right)+\left(L/R\right)\omega_2\end{array}\right)s^3\\+\left(\begin{array}{l}\left(L/R\right)\left(k_{ip}\omega_2-k_{i\omega}\omega_1\right)+\left(1+k_{pq}\right)\left(k_{pp}\omega_2+k_{ip}-k_{p\omega}\omega_1\right)\\+k_{pp}k_{iq}+\alpha\omega_1k_{pq}\dfrac{L}{R}+\left(\left(L/R\right)\omega_2+1\right)k_{iq}+\omega_2\left(1+k_{pq}\right)\end{array}\right)s^2\\+\left(\begin{array}{l}\left(1+k_{pq}\right)\left(k_{ip}\omega_2-k_{i\omega}\omega_1\right)+k_{iq}\left(k_{pp}\omega_2+k_{ip}-k_{p\omega}\omega_1\right)\\+\alpha\omega_1k_{iq}\left(L/R\right)+\omega_2k_{iq}\end{array}\right)s\\+\left(k_{ip}\omega_2-k_{i\omega}\omega_1\right)k_{iq}\end{array}\right)} \tag{15}$$

$$\frac{Q}{Q^*}=\frac{k_{pq}s+k_{iq}}{\left(L/R\right)s^2+\left(1+k_{pq}\right)s+k_{iq}} \tag{16}$$

Equation (15) shows that the transfer function related to the active power of interfaced converter and its reference value are highly dependent on the SG features and its related controllers. The Nyquist diagrams of P/P^* for various low-value inertias are drawn in Fig. 4. As can be seen for the smallest inertia value, the ratio of P/P^* is extremely near to 1 around the reference of the angular frequency that confirms the accurate active power tracking of the proposed SSC in this condition. Also, the aforementioned explanation is true for J_2 with slightly less accuracy.

Instead, for J_3 and J_4, the active power of the SSC is not able to track its reference value as can be seen in Fig. 4. The phase and bode diagrams of P/P^* illustrated in Fig. 5, further confirm the aforementioned discussions. Based on this figure, for two first low-value inertias, the phases of this ratio is near to zero around the reference of the angular frequency. However, this is not valid for the last two values of J_3 and J_4. On the other hand, it is apparently seen from (16) that the reactive power component of the SSC is not concerned with the SG characteristics.

Fig. 6 and Fig. 7 show the effects of various coefficients of the PI controller on the reactive component of the SSC. According to Fig. 6, increasing the coefficients leads to the improvement of the reactive power sharing in the proposed controller as Q/Q^* gets closer to the unit value. The phase diagrams confirm the improvement process as depicted in Fig. 7.

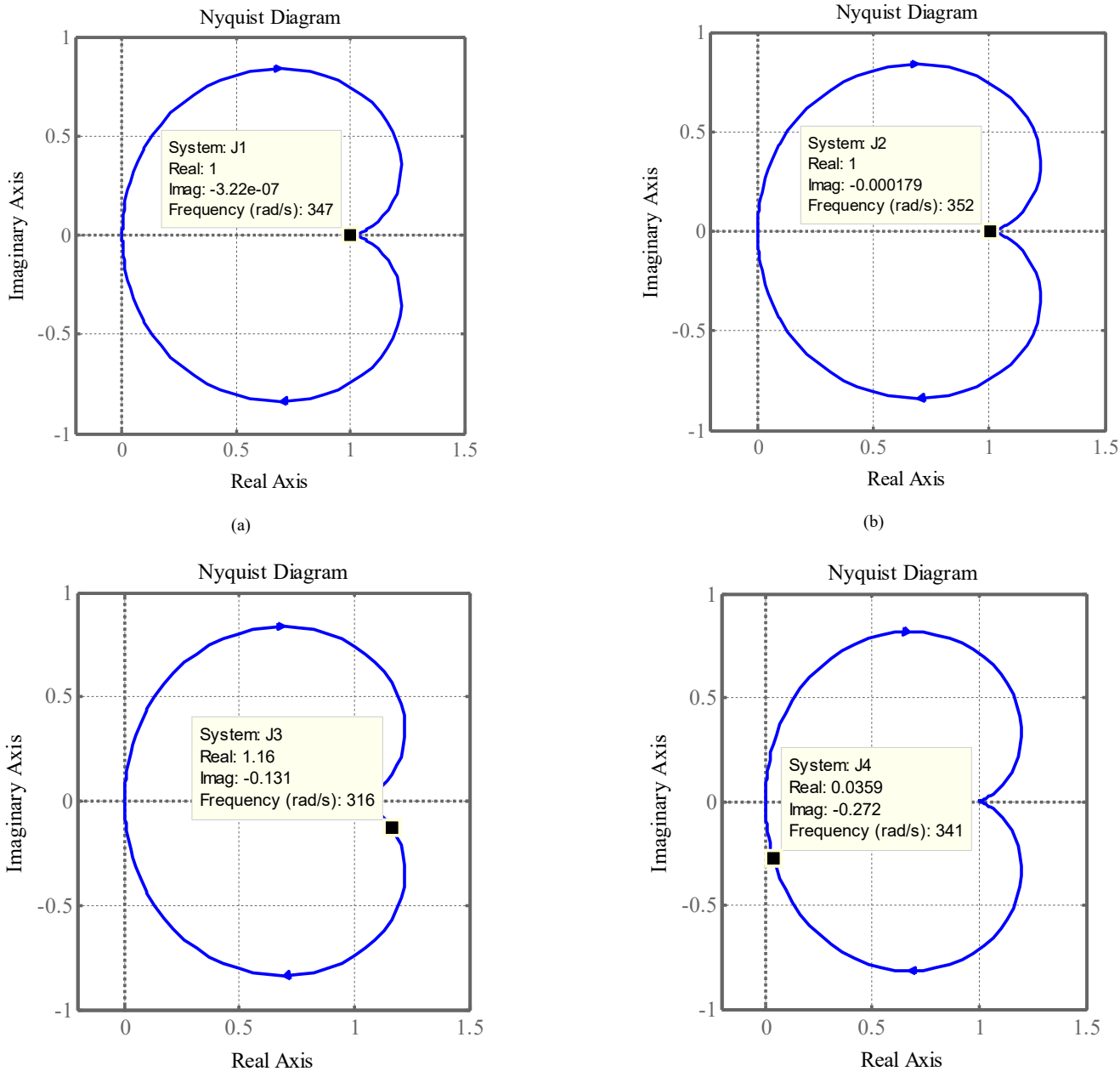

Fig. 4. The Nyquist diagram of P/P^* for different inertia values $J_4>J_3>J_2>J_1$: (a) J_1=8e-8s, (b) J_2=8e-1s, (c) J_3=5s, and (d) J_4=70s.

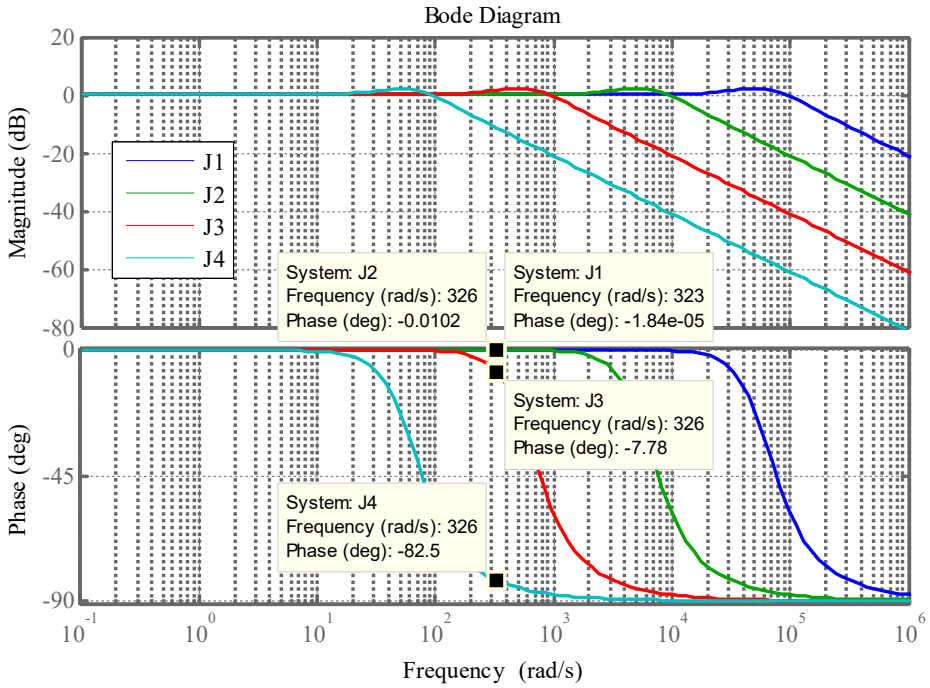

Fig. 5. The phase and bode diagram of P/P^* for various low-value inertias $J_4>J_3>J_2>J_1$, (J_1=8e-8s, J_2=8e-1s, J_3=5s, and J_4=70 s).

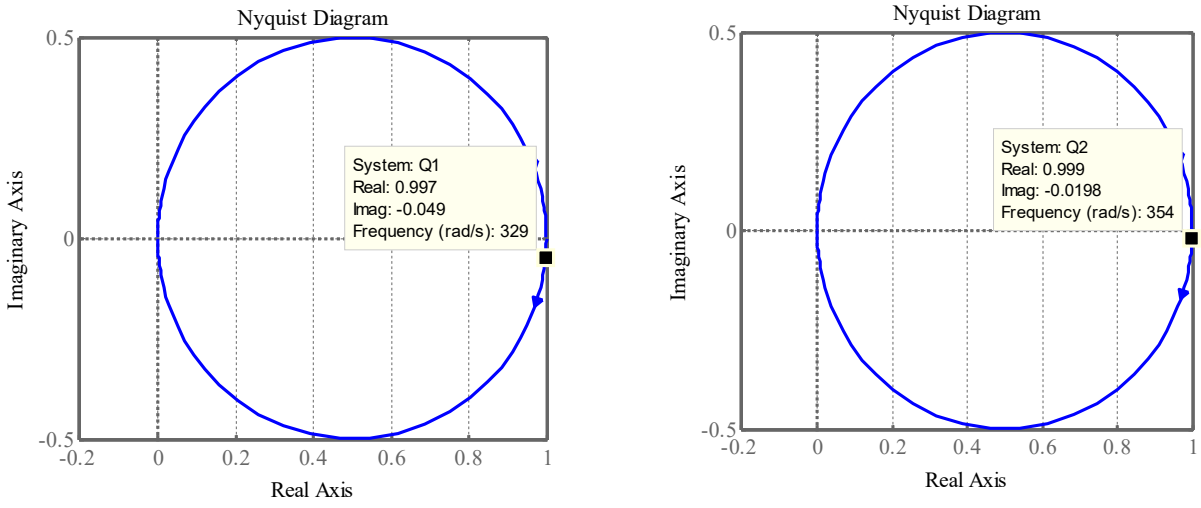

Fig. 6. The Nyquist diagram of Q/Q^* for various coefficients of its related PI controller, (a) k_{pq}=300,k_{iq}=55, and (b) k_{pq}=3000,k_{iq}=550.

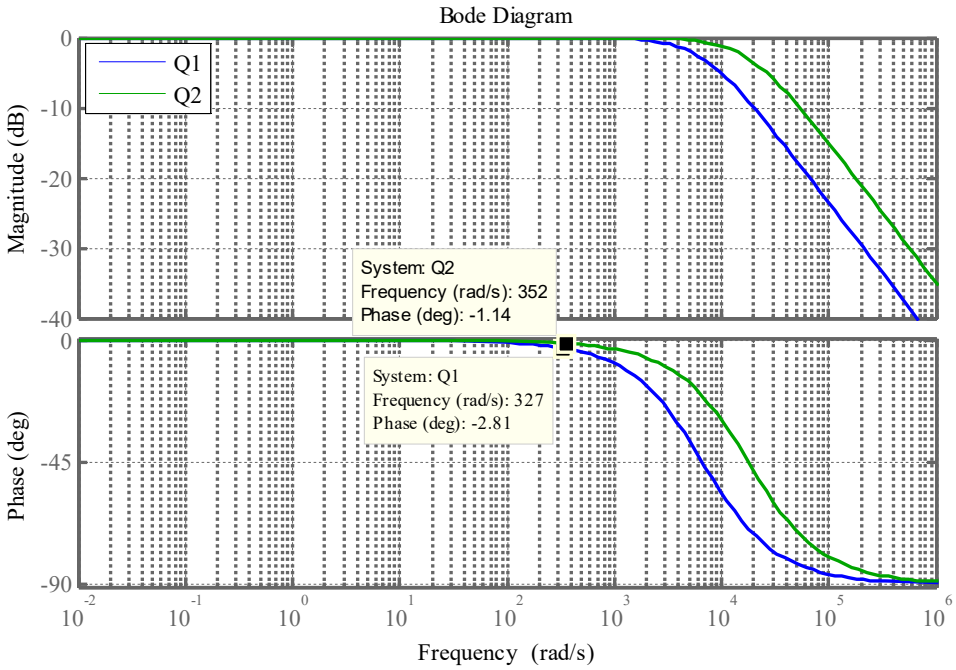

Fig. 7. The phase and bode diagrams of Q/Q* for various coefficients of its related PI controller.

B. The Effects of Active Power Variations on Reactive Power

The active power error can have an impact on the performance of the reactive power sharing in the SSC which is addressed in this subsection. By using the closed-loop diagram shown in Fig. 3, the relation between the reactive power and the active power error can be written as:

$$\frac{Q}{\Delta P}=\frac{-\beta\omega_1(L/R)sP}{\left((L/R)s^3+\left((L/R)\omega_2+1+k_{pq}\right)s^2+\left(\omega_2+k_{iq}+\omega_2 k_{pq}\right)s+\omega_2 k_{iq}\right)} \tag{17}$$

As mentioned in (17), this ratio (Q/ΔP) is also dependent on the active power. By substituting (15) into (17), the effects of active power error can be assessed by the bode diagram presented in Fig. 8 for various inertia values. As can be understood from Fig. 8, for smallest inertia value of J_3, both magnitude and phase values cannot affect the reactive power. Consequently, the SSC is able to damp the negative effects of active power error on reactive power sharing in this operating condition around the reference angular frequency. The reactive power is still affected by the phase due to J_2 in which this value approaches zero because of the generated magnitude as shown in Fig. 8 by the green colour. The worst case is due to J_1. For this inertia value, the magnitude is significantly increased and also the phase is changed in a way that increases the active power error effects and decreases the accuracy of the reactive power sharing.

V. The Evaluation of Virtual Mechanical Power (VMP) Error and Virtual Angular Frequency (VAF) Error Effects

The issues regarding the SG features variations of the SSC are considered in this section. It can be shown that the active and reactive power sharing of the SSC can be noticeably affected by VMP and VAF alterations that these effects can vary under various low-value inertias. The following subsections focus on the mentioned points.

A. The Effects of Virtual Mechanical Power (VMP) Variations

A virtual mechanical power (VMP) variation is contained in the SSC as presented in (13) and (14) in order to simulate the behaviour of the SG in having a synchronous operation of the interfaced converter connected to the power grid. Noticing the SSC, the VMP error can have an impact on both active and reactive power sharing. Thus, the relation between the active power and VMP variation as well as the reactive power and VMP variation can be achieved through Fig. 3 as:

$$P / \Delta P_m = -P / P^* \tag{18}$$

$$\frac{Q}{\Delta P_m} = \frac{\beta\omega_1 (L/R) sP}{\left((L/R)s^3 + \left((L/R)\omega_2 + 1 + k_{pq}\right)s^2 + \left(\omega_2 + k_{iq} + \omega_2 k_{pq}\right)s + \omega_2 k_{iq}\right)} \tag{19}$$

The Root Locus diagrams of (18) and (19) are drawn in Fig. 9 and Fig. 10, respectively. According to Fig. 9, the active power of the SSC can show the stable operation for J_1 around the reference of the angular frequency. However, the SSC cannot make a stable active power for J_2 and J_3; subsequently, this condition causes the active power to be unable to follow its desired value. This scenario is different for $Q/\Delta P_m$. The reactive power can be highly stable for the smallest low-value inertia of J_1 under the presence of VMP variation as shown in Fig. 10. For J_2, a limited stability along with oscillated response is achieved for the reactive power that should be considered in the operation of the SSC. By choosing the J_3 as the highest one in this scenario, the generated reactive power experiences an instability with more fluctuated parts due to the presence of the VMP error in the SSC.

B. The Effects of Virtual Angular Frequency (VAF) Variations

A virtual angular frequency (VAF) based on SG features has been involved in the SSC that can significantly improve the synchronous active and reactive power sharing performance of the interfaced converter. Thus, using the SSC based closed-loop descriptions of active and reactive power as shown in Fig. 3, the active and reactive power transfer functions based on VAF can be obtained as (20) and (21), respectively.

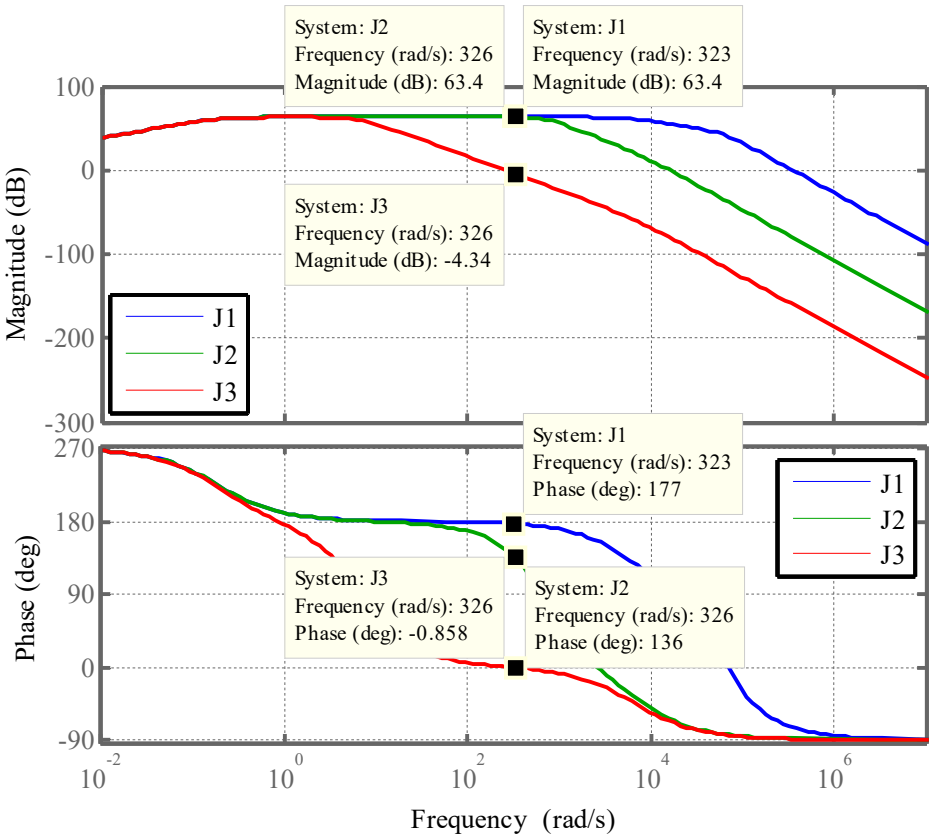

Fig. 8. The bode diagram of Q/ΔP for various low-value inertias J_1>J_2>J_3, (J_3=8e-8s, J_2=8e-1s, and J_1=5s).

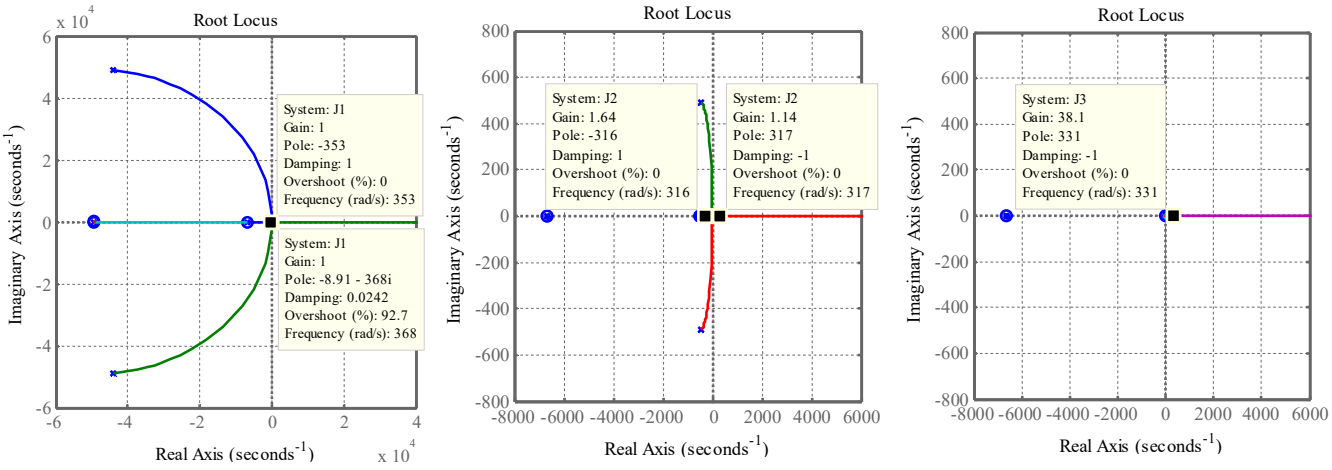

(a) (b) (c)

Fig. 9. The Root Locus diagrams of P/ΔP_m for various low-value inertias J_3>J_2>J_1: (a) J_1=8e-8s (b) J_2=8e-1s and (c) J_3=5s.

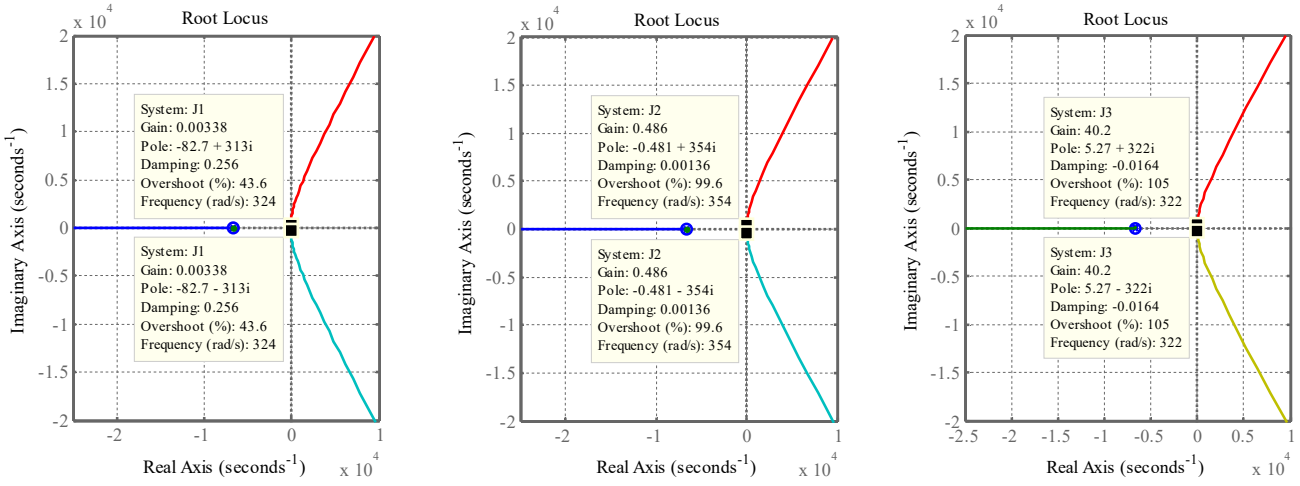

Fig. 10. The Root Locus diagrams of $Q/\Delta P_m$ for various low-value inertias $J_3>J_2>J_1$: (a) J_1==8e-8s (b) J_2=8e-1s and (c) J_3=5s.

Figs. 11 and 12 show the Nyquist diagrams of $P/\Delta\omega$ and $Q/\Delta\omega$ respectively. For two fist smallest inertia values i.e., J_1 and J_2, the effects of VAF variations on active power are very slim around the reference angular frequency meaning that these effects can be neglected as depicted in Fig. 11.

$$\frac{P}{\Delta\omega}=\frac{\begin{pmatrix}k_{p\omega}(L/R)s^4+\begin{pmatrix}(L/R)(k_{i\omega}+k_{p\omega}\omega_2)+\\k_{p\omega}(1+k_{pq})-\alpha(L/R)k_{pq}\end{pmatrix}s^3\\+\begin{pmatrix}k_{i\omega}\omega_2(L/R)+(k_{i\omega}+k_{p\omega}\omega_2)(1+k_{pq})+k_{iq}k_{p\omega}-\\\alpha(L/R)k_{pq}\omega_2-k_{iq}\alpha(L/R)\end{pmatrix}s^2\\+\left(k_{i\omega}\omega_2(1+k_{pq})+k_{iq}(k_{i\omega}+k_{p\omega}\omega_2)-\alpha(L/R)k_{iq}\omega_2\right)s\\+\left(k_{iq}k_{i\omega}\omega_2\right)\end{pmatrix}}{\begin{pmatrix}(L/R)^2s^5+\left((L/R)(2+\omega_2(L/R)+k_{pp}+k_{pq})\right)s^4\\\begin{pmatrix}(L/R)\omega_2+(L/R)(k_{pp}\omega_2+k_{ip})\\+(1+k_{pq})((L/R)\omega_2+1)+k_{pp}(1+k_{pq})+k_{iq}(L/R)\end{pmatrix}s^3\\\begin{pmatrix}(L/R)k_{ip}\omega_2+\omega_2(1+k_{pq})+(k_{pp}\omega_2+k_{ip})(1+k_{pq})\\+k_{iq}(\omega_2(L/R)+1)+k_{iq}k_{pp}+\alpha(L/R)k_{pq}\omega_1\end{pmatrix}s^2\\\begin{pmatrix}k_{ip}\omega_2(1+k_{pq})+k_{iq}\omega_2+k_{iq}(k_{pp}\omega_2+k_{ip})+\\\alpha(L/R)k_{iq}\omega_1\end{pmatrix}s+k_{iq}k_{ip}\omega_2\end{pmatrix}} \tag{20}$$

$$\frac{Q}{\Delta\omega}=\frac{\beta(L/R)s}{(L/R)s^2+(1+k_{pq})s+k_{iq}}P \tag{21}$$

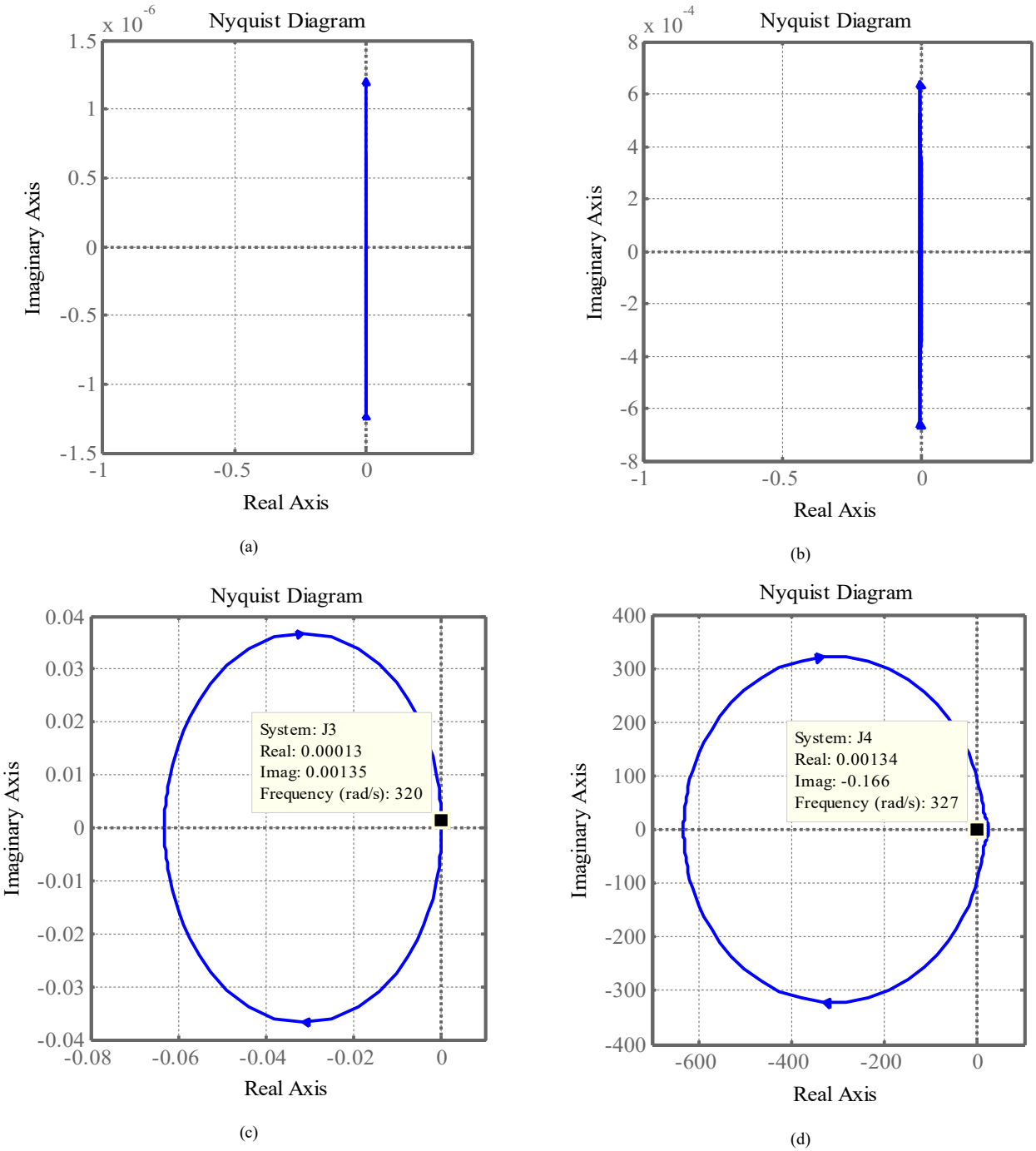

Fig. 11. The Nyquist diagram of P/Δω for different low-value inertias $J_4>J_3>J_2>J_1$: (a) J_1=8e-8s, (b) J_2=8e-1s, (c) J3=5s, and (d) J4=70s.

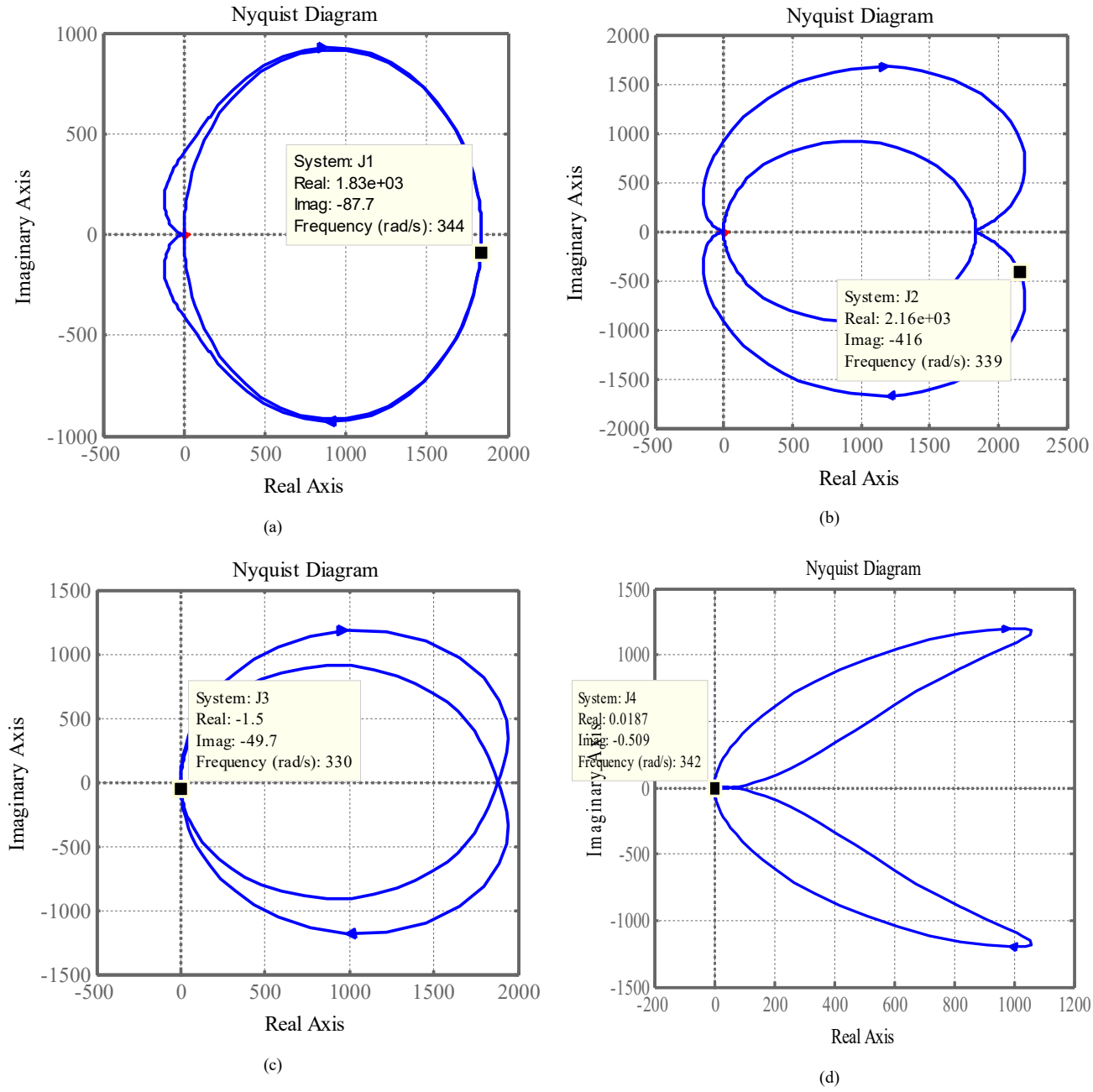

Fig. 12. The Nyquist diagram of Q/Δω for different low-value inertias $J_4>J_3>J_2>J_1$: (a) J1=8e-8s, (b) J2=8e-1s, (c) J3=5s, and (d) J4=70s.

TABLE I

SIMULATION PARAMETERS

Parameter	Value	Parameter	Value
dc-link Voltage (v_{dc})	850 V	J_1	8e-8 s
Phase ac voltage	220 V	P_m with efficiency (η) =90%	3888.9 W
Fundamental frequency	50 Hz	P	3.5 kW
Switching frequency	10 kHz	Q	2.5 kVAR
Interfaced converter resistance	0.1 Ohm	Interfaced converter inductance	45 mH
Power grid resistance	0.1 Ohm	Power grid inductance	0.1 mH
ω_1	39809 rad/s	$k_{p\omega}$	2.512e-5
ω_2	49305 rad/s	$k_{i\omega}$	1.24
k_{pp}	39809	k_{pq}	4000
k_{ip}	19.7e8	k_{iq}	750

In fact, there are no effects due to VAF on active power in this operating condition for the SSC. On the other hand, for the biggest two inertias of J_3 and J_4, the magnitudes of the Nyquist diagrams are very small as shown in Fig. 11. It leads to damping the negative effects of the VAF variation on active power when it exists. But, in comparison with the active power, the reactive power is significantly affected by the VAF variations as shown in Fig. 12. During VAF variation, the SSC based reactive power sharing can be noticeably distorted for the all low-value inertias. However, the effecting process of low-value inertia can be highly decreased in the presence of VAF error for the two last low-value inertias of J_3 and J_4.

VI. Results and Discussions

The proposed model in Fig. 1 has been simulated in MATLAB/SIMULINK environment and performance of the SSC is evaluated under different operating conditions. Distinct values of low-value inertia and virtual mechanical power are considered for the steady state analysis of the SSC. Simultaneous changes of low-value inertia and virtual mechanical power error are extended to ensure the dynamic stability of the SSC during load changes and inverse power flow. The system parameters can be found in Table I.

A. Steady State Operation at Various Inertia Values

The general control diagram of interfaced converter with different low-value inertias under steady-state operating condition is shown in Fig. 13(a). In an initial assessment, the effects of increasing the low-value inertia are investigated as depicted in Fig.14. Fig.14 confirms that all the state variables of the interfaced converter's active and reactive power, voltage magnitude and frequency have accurately followed their reference values for the smallest inertia of J_1=8e-8.

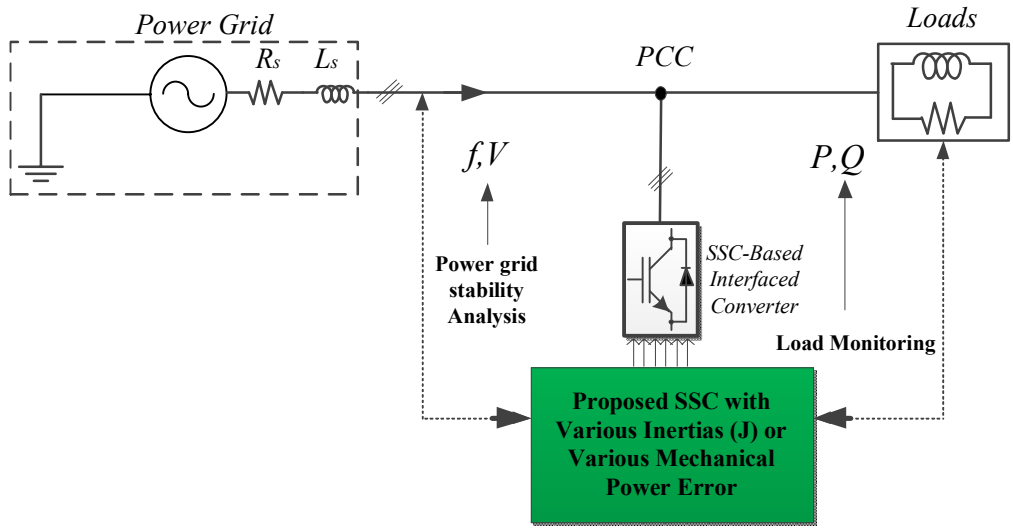

Fig. 13. General structure of the proposed model under steady state condition for different inertias or different virtual mechanical power errors.

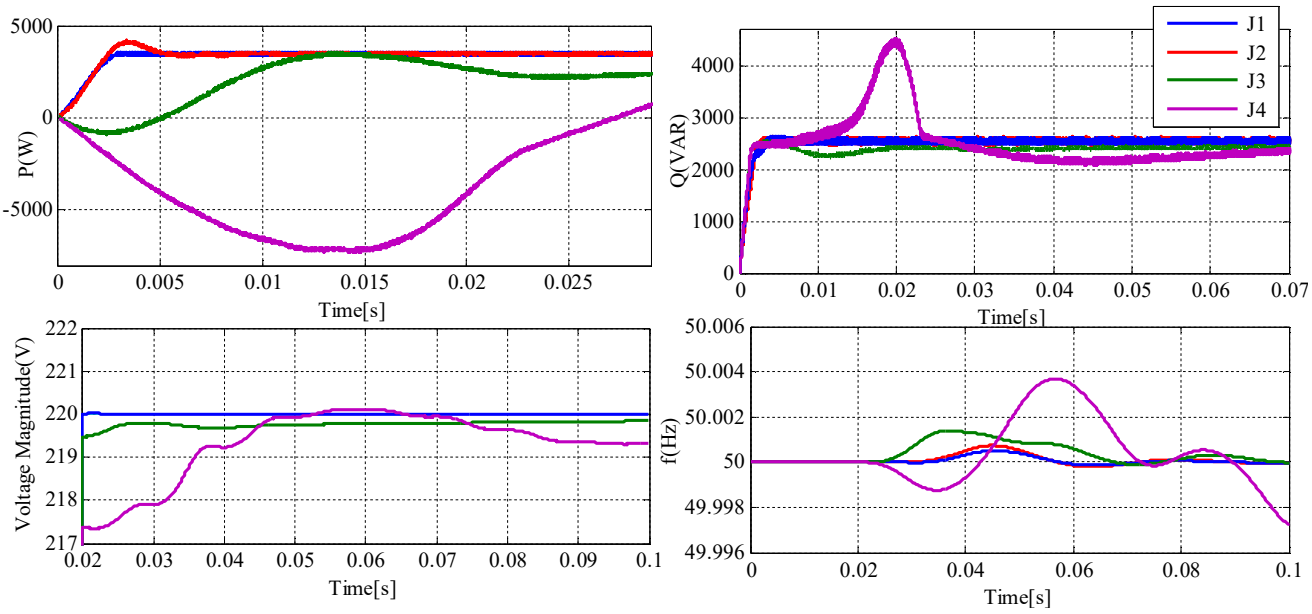

Fig. 14. RER active and reactive power, voltage magnitude and frequency for various low-value inertias ($J_4>J_3>J_2>J_1$) under steady state condition, (J_1=8e-8s, J_2=8e-1s, J_3=5s, and J_4=70s).

According to Fig.14, the best steady state response is associated with interfaced converter active power by the reason of including more elements of SG features in the proposed SSC active component. With the increment of inertia values i.e., J_2, J_3, and J_4, the steady-state responses worsen. The biggest changes that belong to interfaced converter active power and also to the least variations can be observed in the responses of the interfaced converter reactive power. It shows the higher sensitivity of the active component in the proposed controller in comparison with the reactive power. For the two first values of inertia, the stability of the power grid can be achieved as illustrated in Fig.14.

On the other hand, both voltage magnitude and grid frequency become unstable for the highest value of inertia. It confirms the high impact of the proper selection of the low-value inertia in the stability of the power grid with high penetration of RERs by use of the SSC.

B. Steady State Operation with Different Virtual Mechanical Power Errors

Fig. 13(b) shows the overall structure of the proposed controller with various virtual mechanical power errors. The simulation results of this steady state operation of interfaced-converter based RERs system are given in Fig. 15. Based on the proposed SSC, both active and reactive power components of RER are affected by the virtual mechanical power error. Thus, according to Fig. 15, the interfaced converter active and reactive powers will be distorted when virtual mechanical power errors are increased. Using a proportional integral controller for the virtual mechanical power error in the active power component leads to smaller fluctuations of interfaced converter active power in comparison with reactive power as depicted in Fig. 15. The same scenario is valid for voltage magnitude and frequency values. As can be seen in Fig. 15, while the virtual mechanical power error is increased, the voltage magnitude is decreased. This discussion can be stated for the frequency since the overshoot and undershoot responses of the frequency fluctuations are noticeably increased in steady state condition.

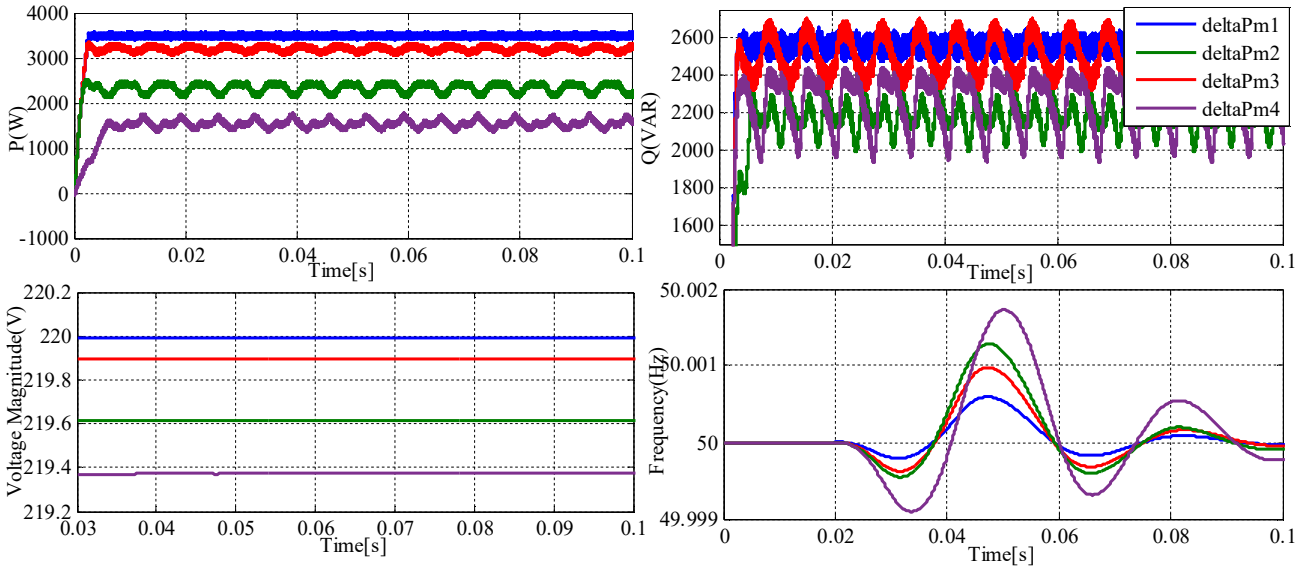

Fig. 15. Active and reactive power of RER, voltage magnitude and frequency for various virtual mechanical power error ($\Delta P_{m4} > \Delta P_{m3} > \Delta P_{m2} > \Delta P_{m1}$).

C. Evaluation of Load Changes

The dynamic evaluation of the SSC during load changes is discussed in this sub-section. An increment of 4.5kW+j2.5kVar is assumed for the initial load connected to the PCC at t=0.1s. Then, after this condition, the SSC-based interfaced converter start to provide the active and reactive power of additional load at t=0.25s. The overall structure of the model in dynamic condition can be seen in Fig. 16. Simultaneous changes of the low-value inertia and virtual mechanical power error are considered in order to guarantee the stable operation of the power grid in load changes condition and analyse the performance of the SSC with various low-value inertias and virtual mechanical power errors.

Fig. 17 illustrates the interfaced converter active and reactive power, voltage magnitude and frequency of the grid under load variations operating condition. The scenario of such a condition is taken into account when the load change takes place at t=0.1 and the SSC doesn't immediately operate. After experiencing the effects of load changes, SSC works at t=0.25. With the first values of (ΔP_{m1}, J_1) shown as blue colour, all variable states of interfaced converter and power grid have their best operation of steady-state and dynamic responses as depicted in Fig. 17. As can be seen, the voltage magnitude of the power grid is noticeably decreased. This drop can be immediately compensated after considering such a load change through the SSC with a fast dynamic response. By analysing the Fig. 17, it can be seen that by simultaneous increment of both low-value inertia and virtual mechanical power error values with the sequences of (ΔP_{m2}, J_2), (ΔP_{m3}, J_3) and (ΔP_{m4}, J_4) drawn as colours of red, green and violet colour respectively, both steady-state and dynamic responses of all state variables start to experience the worst overshoots and undershoots. Among these state variables, the voltage magnitude responses of the power grid include more changes during this increasing process.

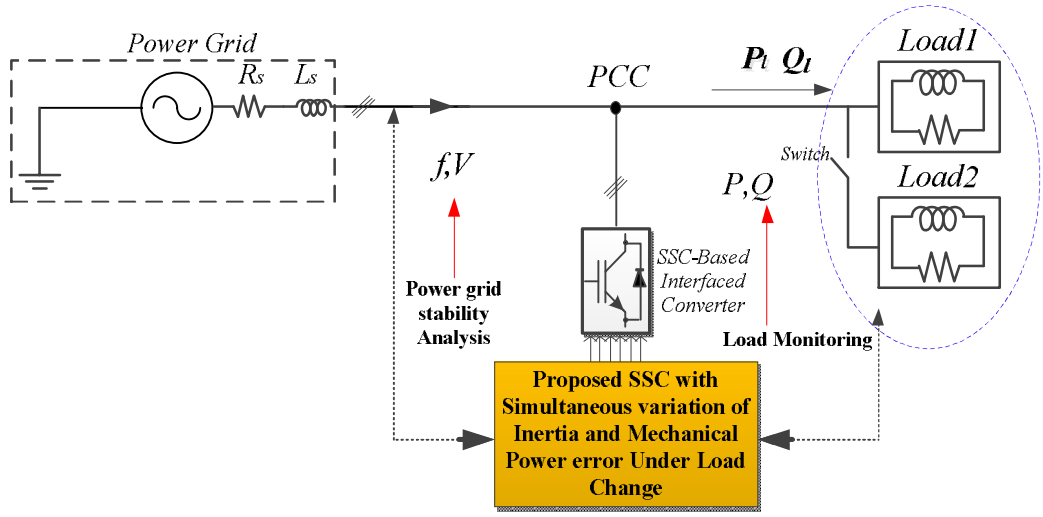

(a)

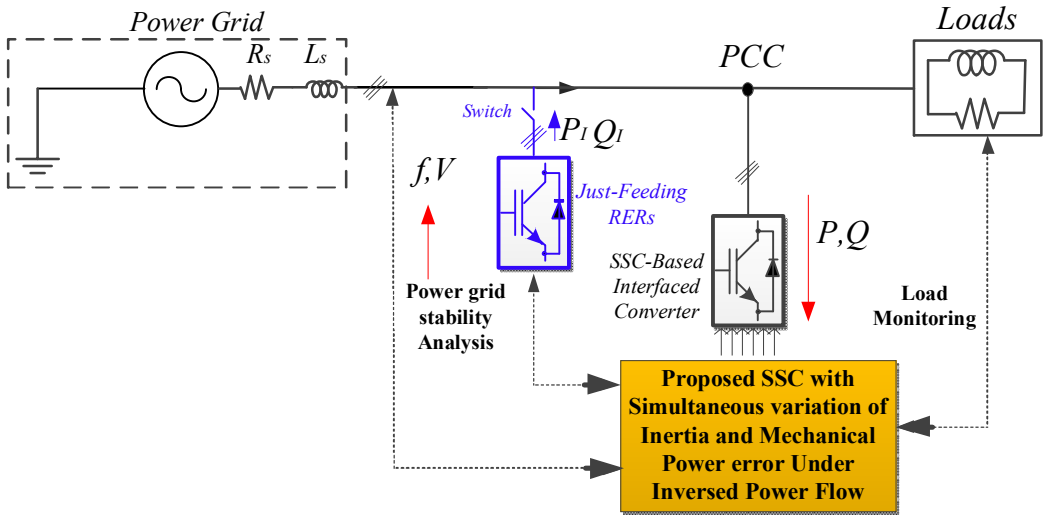

(b)

Fig. 16. General structure of the proposed model with simultaneous variation of inertia and VMP error during: (a) load changes, (b) inverse power flow.

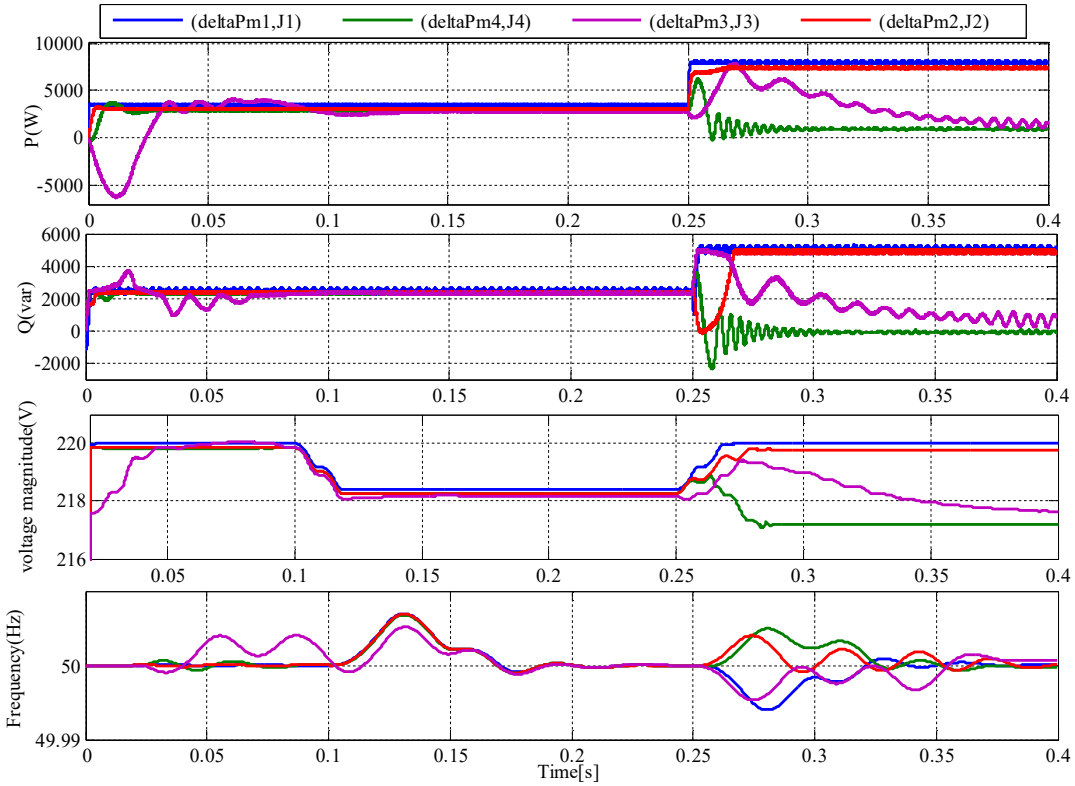

Fig. 17. RER active and reactive power, voltage magnitude and frequency with simultaneous changes of low-value inertia and virtual mechanical power error ($(\Delta P_{m4}, J_4)>(\Delta P_{m3}, J_3)>(\Delta P_{m2}, J_2)>(\Delta P_{m1}, J_1)$) during load changes ($J_1$=8e-8s, J_2=8e-1s, J_3=5s, and J_4=70s).

D. Evaluation of the Inverse Power Flow

Fig. 16(b) shows a high grid-feeding RERs penetration into the power grid considered in this subsection. According to this figure, grid-feeding RERs connected to the PPC at t=0.1s and injects the active and reactive power of 8kW+j4kVar into the grid. In this scenario, the SSC-based RERs is supplying a 13kW+j6kVar grid-connected load. At t=0.25, the SSC-based interfaced converter is governed to decrease its production in order to make stable the power grid against the inverse power flow.

In Fig. 18, the interfaced converter's active and reactive power, voltage magnitude, and frequency with simultaneous changes of low-value inertia and virtual mechanical power error during inverse power flow are illustrated. For the smallest values of low-value inertia and virtual mechanical power error shown as blue colour, the active and reactive power action of the SSC-based interfaced converter is accurately executed in which a very good stable response for both voltage magnitude and frequency of power grid is achieved during both steady state and dynamic operating conditions. By simultaneously increasing inertia and virtual mechanical power error, the unstable and fluctuated responses of all state variables are also increased. The worst responses belong to the highest values (ΔP_{m4}, J_4) that are shown in Fig. 18 through violet colour.

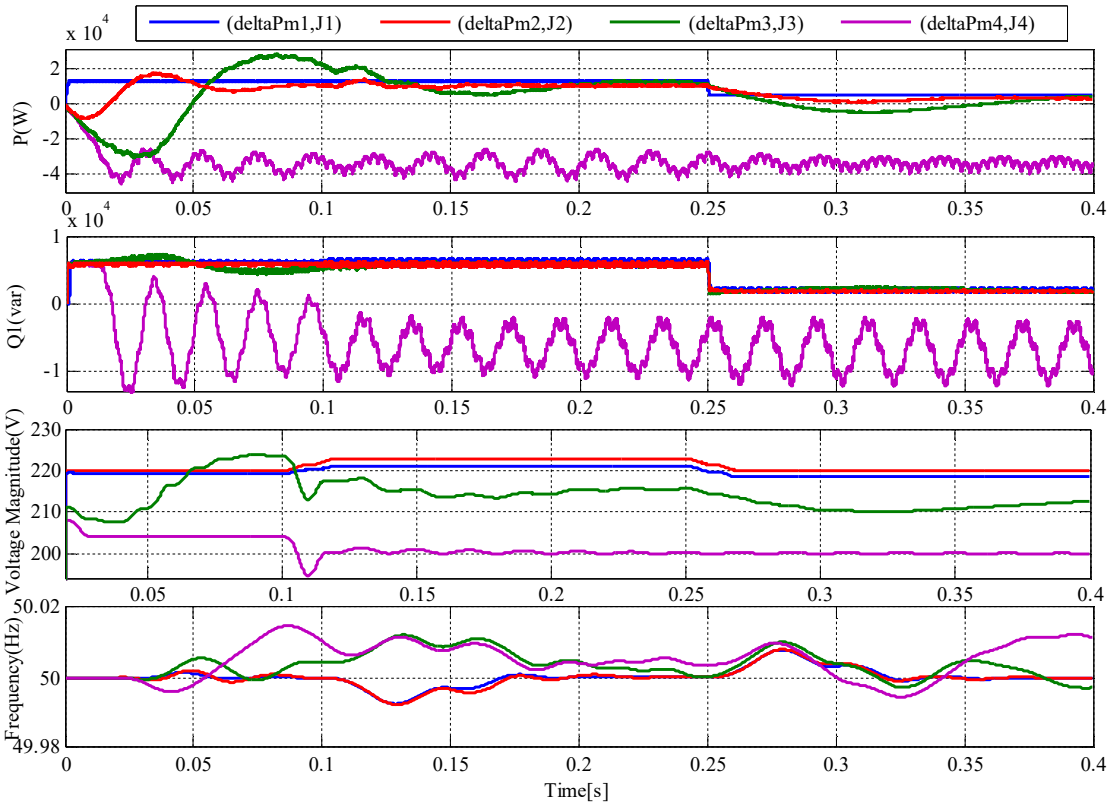

Fig. 18. The RER active and reactive power, voltage magnitude, and frequency during simultaneous changes of low-value inertia and VMP error ((ΔP_{m4}, J_4)>(ΔP_{m3}, J_3)>(ΔP_{m2}, J_2)>(ΔP_{m1}, J_1)) during inverse power flow (J_1=8e-8s, J_2=8e-1s, J_3=5s, and J_4=70s).

E. Comparison with the case of Non-Synchronous Feature

In this subsection, the effects of SGs features embedded in the proposed SSC is discussed. To present more accurate/detailed comparison, the SGs features of the proposed SSC are eliminated at t=0.25s. The results of this comparison are shown in Fig.19. Based on this figure, immediately after eliminating SGs features, all the active power, reactive power, and grid voltage magnitude and frequency become highly unstable and far away from their desired values. As it was predictable, the most change is belonging to active power. It is due to the fact that the active component of proposed SSC consists of more SGs features in comparison with the reactive component. Totally, Fig.19 verifies the importance of considered SGs features in the proposed control technique.

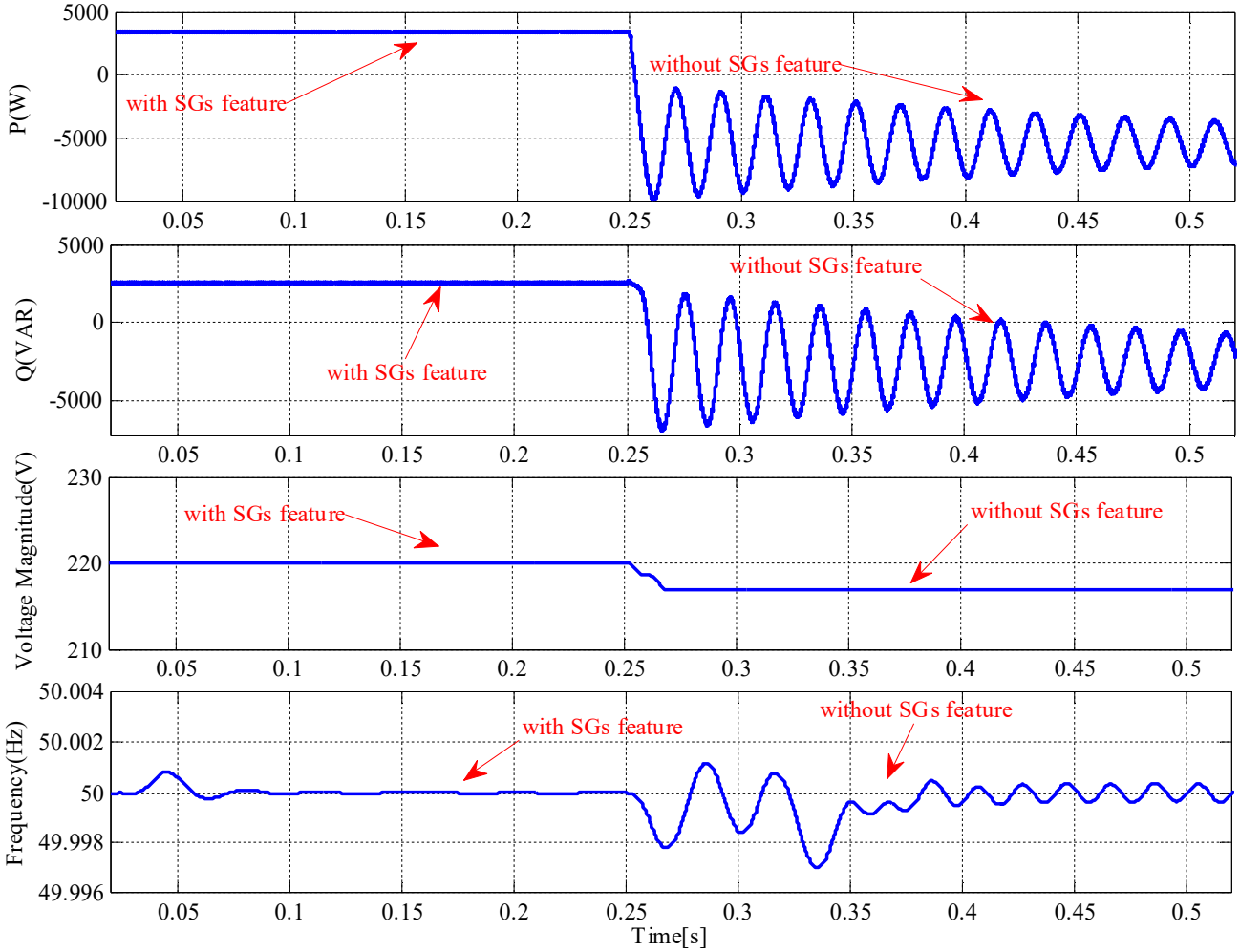

Fig. 19. The RER active and reactive power, voltage magnitude, and frequency with and without SGs feature of proposed SSC.

VII. Conclusion

A single synchronous controller (SSC) has been proposed in this paper for the control of the interfaced converters regarding the large-scale integration of renewable energy resources (RERs) into the power grid. Key features of a synchronous generator (SG), i.e. inertia and mechanical power error were considered in the configuration of the SSC in order to mimic the inherent nature of the SG in employing interfaced converters to provide a stable operation for the power grid with high penetration of RER. Moreover, as the main contribution, the active component of the proposed SSC complies with SG features and enables the proposed SSC-based interfaced converter to demonstrate more accurate mimicry of SG behaviours for generating active power with suitably controllable inertia. Also, both components of the proposed SSC have had no impact on each other due to sufficient decoupling characteristic. Besides, the virtual inertia embedded in the proposed SSC has been ranged widely from very low to high values. An active and reactive power-based dynamic model has been developed and based on it, two closed-loop control diagrams designed in order to analyse the grid stability under different values of SG parameters and used in the SSC. Likewise, the active and reactive power sharing of the interfaced converter as well as power grid stability have been evaluated by employing two transfer functions

formed by the power components and their reference values with various low-value inertias; then, the effects of virtual mechanical power error on active and reactive power sharing has been investigated by two other transfer functions for various low-value inertias. These evaluations have been completed by assessing the impacts of virtual angular frequency (VAF) error on active and reactive power sharing for different low-value inertias. The presented results confirm that by the application of the proposed SSC, the power grid can operate in a stable operating condition even in the presence of large-scale high-penetration renewable energy sources.

Acknowledgment

J.P.S. Catalão acknowledges the support by FEDER funds through COMPETE 2020 and by Portuguese funds through FCT, under SAICT-PAC/0004/2015 (POCI-01-0145-FEDER-016434, ESGRIDS project), 02/SAICT/2017 (POCI-01-0145-FEDER-029803, UNiTED project) and UID/EEA/50014/2019 (POCI-01-0145-FEDER-006961).

References

[1] E. Pouresmaeil, M. Mehrasa, M.A. Shokridehaki, E.M.G. Rodrigues, and J.P.S. Catalão, "Control and stability analysis of interfaced converter in distributed generation technology" *EUROCON 2015*, pp. 1-6, Nov. 2015.

[2] M. Mehrasa, M. E. Adabi, E. Pouresmaeil, and J. Adabi, "Passivity-based control technique for integration of DG resources into the power grid," *Int. Jou. of Electric Power Systems Research*, vol. 58, pp. 281-290, Jan. 2014.

[3] E. Alegria, T. Brown, E. Minear, and R. H. Lasseter, "CERTS microgrid demonstration with large-scale energy storage and renewable generation," *IEEE Trans. Smart Grid*, vol. 5, no. 2, pp. 937–943, Mar. 2014.

[4] P. Harsha and M. Dahleh, "Optimal management and sizing of energy storage under dynamic pricing for the efficient integration of renewable energy," *IEEE Trans. Power Syst.*, vol. 30, no. 3, pp. 1164–1181, May 2015.

[5] S. Wang et al., "Design and advanced control strategies of a hybrid energy storage system for the grid integration of wind power generations," *IET Renew. Power Generation*, vol. 9, no. 2, pp. 89–98, Mar. 2015.

[6] S. Liu, X. Wang, and P. X. Liu, "A Stochastic Stability Enhancement Method of Grid-Connected Distributed Energy Storage Systems," *IEEE Trans. Smart Grid*, DOI: 10.1109/TSG.2015.2514286. 2017.

[7] T. Stetz, F. Marten, and M. Braun, "Improved low voltage grid-integration of photovoltaic systems in Germany," *IEEE Trans. Sustain Energy*, vol. 4, no. 2, pp. 534 - 542, June. 2012.

[8] E. Demirok, P. C. Gonzalez, K. Frederiksen, D. Sera, P. Rodriguez, and R. Teodorescu, "Local reactive power control methods for overvoltage prevention of distributed solar inverters in low-voltage grids," *IEEE J. Photovoltaics*, vol. 1, no. 2, pp. 174–182, Oct. 2011.

[9] A. Yazdani, A. Di Fazio, H. Ghoddami, M. Russo, M. Kazerani, J. Jatskevich, K. Strunz, S. Leva, and J. Martinez, "Modeling guidelines and a benchmark for power system simulation studies of three-phase single-stage photovoltaic systems," *IEEE Trans. Power Del.*, vol. 26, no. 2, pp. 1247–1264, Apr. 2011.

[10] A. Samadi, R. Eriksson, L. Söder, B. G. Rawn, and J.C. Boemer, "Coordinated Active Power-Dependent Voltage Regulation in Distribution Grids With PV Systems," *IEEE Trans. Power Del.*, vol. 29, no. 3, pp. 1454–1464, Jun. 2014.

[11] S. D. Arco and J. A. Suul, "Equivalence of virtual synchronous machines and frequency-droops for converter-based microgrids," *IEEE Trans. Smart Grid*, vol. 5, no. 1, pp. 394–395, Jan. 2014.

[12] M. Mehrasa, E. Pouresmaeil, B. Pournazarian, A. Sepehr, M. Marzband, and J.P.S. Catalão, "Synchronous Resonant Control Technique to Address Power Grid Instability Problems Due to High Renewables Penetration," Energies, vol. 11, no. 9, pp. 2469, Sep. 2018.

[13] H. Alatrash, A. Mensah, E. Mark, G. Haddad, and J. Enslin, "Generator emulation controls for photovoltaic inverters," *IEEE Trans. Smart Grid*, vol. 3, no. 2, pp. 996–1011, Jun. 2012.

[14] M. Mehrasa, R. Godina, E. Pouresmaeil, I. Vechiu, R. L. Rodríguez, and J.P.S. Catalão, "Synchronous active proportional resonant-based control technique for high penetration of distributed generation units into power grids," IEEE PES Innovative Smart Grid Technologies Conference Europe (ISGT-Europe), pp. 1-6, Jan. 2018.

[15] M. A. Torres, L. A. Lopes, L. A. Moran, and J. R. Espinoza, "Self-tuning virtual synchronous machine: A control strategy for energy storage systems to support dynamic frequency control," *IEEE Trans. Energy Convers*., vol. 29, no. 4, pp. 833–840, Dec. 2014.

[16] L. Zhang, L. Harnefors, and H-P. Nee, "Power-Synchronization Control of Grid-Connected Voltage-Source Converters," *IEEE Transactions on Power Systems*, vol.25, no.2, pp.809-820, May 2010.

[17] M.P.N.V. Wesenbeeck, S.W.H. D Haan, P.Varela, and K. Visscher, "Grid Tied Converter with Virtual Kinetic Storage," *PowerTech*, pp.1-7, July 2009.

[18]W. Zhang, A. M. Cantarellas, J. Rocabert, A. Luna, and P. Rodriguez, "Synchronous Power Controller With Flexible Droop Characteristics for Renewable Power Generation Systems," *IEEE Trans. Sustainable Energy*, vol. 7, pp. 1572-1582, Oct. 2016.

[19]M. Chamana, B. H. Chowdhury, and F. Jahanbakhsh, "Distributed Control of Voltage Regulating Devices in the Presence of High PV Penetration to Mitigate Ramp-Rate Issues," *IEEE Trans. Smart Grid*, in press.

[20] Q. C. Zhong, P. Nguyen, Z. Ma, and W. Sheng, "Self-synchronized synchronverters: Inverters without a dedicated synchronization unit," *IEEE Trans. Power Electron.*, vol. 29, no. 2, pp. 617–630, Feb. 2014.

[21] S. D. Arco and J. A. Suul, "Virtual synchronous machines—Classification of implementations and analysis of equivalence to droop controllers for microgrids," in Proc. *Power Tech* 2013, pp. 1–7.

[22] W. Zhang, D. Remon, A. Mir, A. Luna, J. Rocabert, I. Candela, and P. Rodriguez "Comparison of Different Power Loop Controllers for Synchronous Power Controlled Grid-Interactive Converters," in Proc. *ECCE*, pp. 3780–3787, Oct. 2015.

[23] S. D'Arco, J. A. Suul, and O. B. Fosso, "A Virtual Synchronous Machine Implementation for Distributed Control of Power Converters in SmartGrids," *Electric Power System Research*, vol. 122, pp. 180-197, May 2015.

[24] S. D'Arco, J. A. Suul, and O. B. Fosso, "Small-Signal Modeling and Parametric Sensitivity of a Virtual Synchronous Machine," in Proceedings *PSCC*, Wrocław, Poland, Aug. 2014.

[25] S. D'Arco, J. A. Suul, and O. B. Fosso, "Control System Tuning and Stability Analysis of Virtual Synchronous Machines," in Proceedings *ECCE* 2013, Denver, Colorado, USA, pp. 2664-2671.

[26] Q. C. Zhong and G. Weiss, "Synchronverters: Inverters that mimic synchronous generators," *IEEE Trans. Ind. Electron*., vol. 58, no. 4, pp. 1259–1267, Apr. 2011.

[27] Y. Ma, W. Cao, L. Yang, F. (Fred) Wang, and L. M. Tolbert, " Virtual Synchronous Generator Control of Full Converter Wind Turbines with Short-Term Energy Storage", *IEEE Transactions on Industrial Electronics*, vol: 64 (11), pp. 8821 - 8831, Nov. 2017.

[28] J. Liu, Y. Miura, and T. Ise, "Comparison of Dynamic Characteristics Between Virtual Synchronous Generator and Droop Control in Inverter-Based Distributed Generators", *IEEE Trans. Pow. Electron*, vol:31(5), pp. 3600-3611, May. 2016.

[29] M. Guan, W. Pan, J. Zhang, Q. Hao, J. Cheng, and X. Zheng, "Synchronous Generator Emulation Control Strategy for Voltage Source Converter (VSC) Station', *IEEE Trans. Pow. System*, vol:30 (6), pp. 3093-3101, Nov 2015.